

Two-particle spectral function for disordered s-wave superconductors: local maps and collective modes

Abhisek Samanta¹, Amulya Ratnakar², Nandini Trivedi³ and Rajdeep Sensarma¹

1. *Department of Theoretical Physics, Tata Institute of Fundamental Research, Mumbai 400005, India.*

2. *UM-DAE Centre for Excellence in Basic Sciences, Mumbai University, Mumbai, India*

3. *Physics Department, The Ohio State University, Columbus, Ohio, USA 43201*

(Dated: June 6, 2018)

We make the first testable predictions for the *local two-particle* spectral function of a disordered s-wave superconductor, probed by scanning Josephson spectroscopy (sjs), providing complementary information to scanning tunneling spectroscopy (sts). We show that sjs provides a direct map of the local superconducting order parameter that is found to be anticorrelated with the gap map obtained by sts. Furthermore, this anticorrelation increases with disorder. For the momentum resolved spectral function, we find the Higgs mode shows a non-dispersive subgap feature at low momenta, spectrally separated from phase modes, for all disorder strengths. The amplitude-phase mixing remains small at low momenta even when disorder is large. Remarkably, even for large disorder and high momenta, the amplitude-phase mixing oscillates rapidly in frequency and hence do not affect significantly the purity of the Higgs and phase dominated response functions.

Introduction: Superconductivity, characterized by a macroscopic complex wavefunction of Cooper pairs, can be destroyed along two distinct routes: (a) by reducing the amplitude of the wavefunction to zero, as observed in conventional clean superconductors at T_c , where Cooper pairs break apart, or (b) by disordering the phase of the wavefunction, while keeping the pairing amplitude finite, as seen in strongly interacting [1–3], or in strongly disordered superconductors [4–7].

There is strong experimental [8–10] and theoretical [5–7, 11, 12] evidence that the destruction of superconductivity in thin films at high disorder [13–15] is driven by loss of phase coherence of Cooper pairs, whereas the single particle fermionic spectrum remains gapped through the superconductor to insulator transition. The low energy excitations of this system are the dynamical fluctuations of the amplitude (Higgs) and phase (Goldstone) modes of the complex order parameter. The Higgs mode in superconductors has been studied experimentally using optical [16] and Raman [17] spectroscopy. It has also been studied in neutral ultracold atomic systems through lattice modulation spectroscopy [18]. In disordered superconductors, recent experiments [10] have interpreted low energy optical absorption as indicative of absorption by Higgs modes within the single particle gap.

While the claim of observing pure amplitude Higgs modes in ultracold atoms is undeniable, there are two main issues that prevent current experiments on quantum materials from reaching similar unambiguous conclusions: (a) Materials are inherently disordered so it is not evident to what extent the low energy absorption can be separated into pure phase and amplitude (Higgs) modes in systems with broken translational symmetry. This is one of the key questions we address and answer in this article. (b) The experiments currently do not have direct access to a spatial map of the inhomogeneous superconducting order parameter in the disordered systems. A systematic study of the evolution of collective modes with disorder is required to resolve these issues.

Main results: In this work, we use a non-perturbative functional integral approach [19] to trace the evolution of the two-

particle collective spectrum of a disordered attractive Fermi Hubbard model. We present for the first time the full momentum and frequency dependence of the disorder averaged spectral function as well as spectral function maps in real space for a given disorder realization. Our spectral function maps at large disorder show strong correlation between superconducting patches and low energy pair spectral weight, which are found to be anticorrelated with regions of large local gap. We thus make testable predictions for scanning tunneling [20] and scanning Josephson spectroscopies [21] for the first time.

From our theoretical approach we can easily separate the contribution of the amplitude (Higgs) modes, the phase modes and the amplitude-phase mixing. We therefore obtain key insights into the relative importance of the mixing contributions in different spectral regions and for different degrees of disorder. We find that the local response is dominated by the phase modes, while the Higgs and amplitude-phase mixing contributions play a subdominant role. An intriguing feature of the spatial maps of the amplitude-phase mixing contribution is its oscillatory nature over length scales much shorter than the superconducting patches. Since the tunneling probes average over a few lattice spacings, we expect the mixing to not be important.

The momentum-dependent spectral functions show two features important for understanding the experiments: (a) At arbitrarily low disorder, the Higgs modes at low momenta form non-dispersive states below the two particle threshold that are spectrally separated from the low energy phase modes. This subgap feature persists with increasing disorder and is predominantly made of Higgs fluctuations with small amplitude-phase mixing. Thus, we expect experiments observing subgap features at finite frequency are indeed probing the Higgs modes of the disordered system. (b) The amplitude phase mixing at higher momenta show a dramatic evolution with disorder. At low disorder it is predominantly of one sign, while at larger disorder, it oscillates and changes sign rapidly as a function of frequency. Thus, we expect that high disorder, temperature, or finite resolution broadening of

spectroscopic probes, will washout the effects of amplitude-phase mixing, a result that is rather counter-intuitive. In summary, our work makes testable predictions for experiments and provides a bridge between microscopic models that start with fermionic degrees of freedom [5, 6] and effective bosonic models [4, 22].

Model and Methods: We analyze the behavior of the disordered attractive Hubbard model on a square lattice using an inhomogeneous self-consistent functional integral approach. The Hamiltonian is given by:

$$H = -t \sum_{\langle rr' \rangle \sigma} c_{r\sigma}^\dagger c_{r'\sigma} - U \sum_r n_{r\uparrow} n_{r\downarrow} + \sum_r v_r n_r \quad (1)$$

where $c_{r\sigma}^\dagger$ ($c_{r\sigma}$) is the creation (annihilation) operator for electrons with spin σ on site r , t is the nearest-neighbour hopping, and $|U|$ is the attractive interaction leading to Cooper pairing. Here, v_r is a random potential, drawn independently for each site from a uniform distribution of zero mean and width V , where V sets the scale of disorder in the problem.

Within our approach, the mean field theory is the saddle point of the fermionic action, described by static local Cooper pairing field $\Delta_0(r) = \langle c_{r\uparrow}^\dagger c_{r\downarrow}^\dagger \rangle$ and the Hartree shift $\xi_0(r) = U \langle c_{r\sigma}^\dagger c_{r\sigma} \rangle$, determined self-consistently. We expand the action around this saddle point by considering a fluctuating pairing field $\Delta(r, \tau) = (\Delta_0(r) + \eta(r, \tau)) e^{i\theta(r, \tau)}$ upto quadratic order, where η and θ correspond to the amplitude and phase fluctuations of the order parameter, and obtain,

$$\begin{aligned} \mathcal{P}_{11}(r, r', \omega) &= -\frac{1}{\pi} \text{Im} \langle \eta(r, \omega + i0^+) \eta(r', -\omega + i0^+) \rangle \\ \mathcal{P}_{12}(r, r', \omega) &= -\frac{1}{\pi} \text{Im} \langle \eta(r, \omega + i0^+) \theta(r', -\omega + i0^+) \rangle \\ \mathcal{P}_{22}(r, r', \omega) &= -\frac{1}{\pi} \text{Im} \langle \theta(r, \omega + i0^+) \theta(r', -\omega + i0^+) \rangle \end{aligned} \quad (2)$$

where \mathcal{P}_{11} is the spectral density of amplitude fluctuations, \mathcal{P}_{22} that of phase fluctuations and \mathcal{P}_{12} is the amplitude-phase mixing term [23] [See SM for details].

While η and θ are the natural choice of fluctuation co-ordinates, experimental probes, which couple to the fermion density or current, always couple to $\Delta_0(r) e^{i\theta(r, \tau)} \sim i\Delta_0(r)\theta(r, \tau)$. The two particle correlation function, measurable by Josephson spectroscopy, is $P(r, r', \omega) = \sum_{\alpha\beta} P_{\alpha\beta}(r, r', \omega)$, where $P_{11} = \mathcal{P}_{11}$, $P_{12}(r, r', \omega) = \Delta_0(r)\mathcal{P}_{12}(r, r', \omega)$, $P_{21}(r, r', \omega) = \Delta_0(r')\mathcal{P}_{21}(r, r', \omega)$ and $P_{22}(r, r', \omega) = \Delta_0(r)\Delta_0(r')\mathcal{P}_{22}(r, r', \omega)$. We will now consider the evolution of these experimentally measurable spectral functions with disorder.

Local pair spectral function: In a mean field description, the system breaks up into superconducting and insulating islands at intermediate and large disorder [5]. STM measurements also show indirect evidence of strong spatial inhomogeneity in patchy single particle gap-maps [20]. However, a direct access to the inhomogeneous superconducting order parameter is missing in these systems. We find that the inte-

grated local two-particle spectral weight is strongly spatially correlated with the superconducting order parameter and further shows strong anti-correlation with local single particle gaps. Our prediction can be experimentally tested by combining scanning tunneling with scanning Josephson spectroscopy data [21].

In Fig. 1(a) and (b), we show the local order parameter $\Delta_0(r)$ and the integrated local 2-particle spectral weight $F(r) = \int_0^{2E_{gap}} P(r, r, \omega)$ for a typical configuration at large disorder ($V = 6$) [24]. We notice the strong spatial correlation between regions with large $\Delta_0(r)$ and large $F(r)$. Although regions with small $\Delta_0(r)$ have small phase stiffness, these phase fluctuations do not contribute to the pair spectral function as $\Delta_0(r)$ is small in these regions. We have checked that this strong correlation is robust to choice of disorder configurations and to variation of cutoffs used to calculate $F(r)$ [See SM for details]. The integrated spectral weight can thus be used to experimentally map out the superconducting regions in the system. In Fig. 1(c), we plot the local single particle gap $E(r)$, obtained from peaks in the local one particle density of states for the same configuration [See SM for details]. The maps in Fig. 1 (a) and (b) shows strong spatial anti-correlation between regions with large $\Delta_0(r)$ or $F(r)$ and regions with large $E(r)$, i.e. large single particle gaps map out the insulating regions in the system. To track the evolution of this strong anti-correlation between $F(r)$ and $E(r)$, in Fig. 1(d), we plot the covariance of these quantities, averaged over disorder configurations, as a function of V . The negative correlations increase with disorder, as the system breaks up into superconducting and non-superconducting regions.

The relative contribution of the Higgs mode (P_{11}), phase mode P_{22} , and the amplitude-phase mixing ($P_{12} + P_{21}$) to the 2-particle spectral function is a key question of interest, especially in the light of papers with contradictory claims on this matter [8, 11, 25, 26]. In Fig. 1(e) we plot $F_{11} + F_{22}$ as bars on each lattice site with the contribution from F_{22} shown in red and that from F_{11} shown in yellow. We find that the local 2-particle spectral weight is dominated by the phase modes, with the amplitude and mixing contributions playing a sub-leading role. The contribution of the mixing, $F_{12} + F_{21}$ is plotted as a map in Fig. 1(f). P_{12} and P_{21} does not have the interpretation of a spectral weight and changes from positive to negative over different regions in the map. Hence, while mixing plays a somewhat important but subleading role in the local spectral weight, it should have minimal impact on the signals in probes which look at spatially averaged quantities.

Momentum and energy dependence of collective modes: We now consider the spectral function $P_{\alpha\beta}(q, \omega) = \sum_{rr'} e^{iq \cdot (r-r')} P_{\alpha\beta}(r, r', \omega)$ (after disorder averaging) to study the behaviour of the collective modes. In the optical conductivity the pair spectral function contributes to loop corrections, hence their effect cannot be spectrally resolved. A more direct momentum and frequency resolved measurement is possible with the recently developed M-EELS techniques [27]. Fig. 2(a)-(d) shows the Higgs spectral function

$P_{11}(q, \omega)$ with increasing disorder. For $V = 0$, a Goldstone mode exists, but the Higgs contribution to the spectral weight vanishes as $q \rightarrow [0, 0]$. The picture changes dramatically even for a weak disorder of $V = 0.1t$, where the Higgs mode develops finite weight at the zone center at an energy well below the two-particle continuum threshold. We have checked that this phenomenon exists even at a weaker disorder of $V = 0.05$. The relatively flat dispersion of the Higgs mode suggests localization of these modes at a finite energy. With increasing disorder the Higgs mode flattens and broadens, with the threshold for the mode decreasing with disorder. The Higgs threshold is plotted as a function of disorder in Fig. 2(i). It does not follow the continuum threshold ($2E_{gap}$) even at low disorder. We also observe a pile up of low energy weight at the commensurate M point ($[\pi, \pi]$) at intermediate disorder of $V = 1.0$, indicating fluctuating pair-density waves, although there is no zero energy weight and static order is absent in the mean-field theory.

We now focus on the phase contribution to the spectral function $P_{22}(q, \omega)$ in Fig 2 (e)-(h). The linearly dispersing collective mode at low q broadens with disorder, and the dispersion becomes flatter. The dispersive mode can be identified even for large disorder $V \approx 5t$. The speed of sound, extracted from the slope of the dispersion, is plotted in Fig. 2 (i). It decreases with disorder, going to zero near $V \approx 5.5t$. It is also evident from the color-scales that phase fluctuations dominate over amplitude fluctuations in the entire disorder range. Finally, in Fig 2 (j)-(l), we plot the mixing term $P_{12}(q, \omega) + P_{21}(q, \omega)$, as a function of q and ω for increasing disorder. It is evident that with increasing disorder the mixing term rapidly oscillates between positive and negative values as a function of the frequency and hence mixing terms give small contributions to the pair spectral function.

The clear dominance of the phase modes over Higgs modes leads to the question whether the interesting features of the Higgs spectral function can be visible in experiments. Fortunately, the features of the Higgs and the phase spectral functions are well separated in energy at low q and hence probes which couple to the spatially averaged pair spectral function in an energy resolved manner should see these features clearly (see Fig 3(a)-(f)). It is important to note that this spectral separation is a feature of low q response and is not present in the local response we investigated in the previous section. We also find that the amplitude-phase mixing term has negligible contribution at all frequencies near $q = 0$, and the relative contribution decreases with disorder, contrary to the popular belief that they are the dominant force in shaping the collective spectrum. This can be understood from the fact that the mixing contribution varies from positive to negative values in space, as seen in Fig. 1(f), and hence averages to zero when one looks at low q response of the system.

Discussion: We have investigated the evolution of collective modes in a disordered s-wave superconductor starting from a microscopic description. We find that the local 2-particle spectral weight is strongly correlated with the superconducting regions and strongly anti-correlated with regions

of high one particle spectral gap. The pair response is dominated by the phase mode, but the Higgs mode shows interesting features at low q which are spectrally separated from the phase mode contributions. The amplitude phase mixing term plays a subdominant role at large disorder due to rapid change of sign.

The authors thank P. Raichaudhuri for useful discussions. A.S., A.R. and R.S. acknowledge computational facilities at the Department of Theoretical Physics, TIFR Mumbai. N.T. acknowledges funding from grant NSF-DMR-1309461.

-
- [1] Lee, P. A., Nagaosa, N. & Wen, X. Doping a Mott insulator: Physics of high-temperature superconductivity. *Rev. Mod. Phys.* **78**, 17 (2006).
 - [2] Anderson, P. W., Lee, P. A., Randeria, M., Rice, T. M., Trivedi, N. & Zhang, F. C. The physics behind high-temperature superconducting Cuprates : the 'plain vanilla' version Of RVB. *J Phys. Condens. Matter* **16**, R755 (2004).
 - [3] Melo, C. A. R. Sa de, Randeria, M. & Engelbrecht, J. R. Crossover from BCS to Bose superconductivity : Transition temperature and time-dependent Ginzburg-Landau Theory. *Phys. Rev. Lett.* **71**, 3202 (1993).
 - [4] Fisher, M. P. A., Weichman, P. B., Grinstein, G. & Fisher, D. S. Boson localization and the superfluid-insulator transition. *Phys. Rev. B* **40**, 546570 (1989).
 - [5] Ghosal, A., Randeria, M. & Trivedi, N. Inhomogeneous pairing in highly disordered s-wave superconductors. *Phys. Rev. B* **65**, 014501 (2001).
 - [6] Bouadim, K., Loh, Y. L., Randeria, M. & Trivedi, N. Single- and two-particle energy gaps across the disorder-driven superconductor-insulator transition. *Nature Physics* **7**, 884-889 (2011).
 - [7] Trivedi, N., Scalettar, R. T., & Randeria, M. Superconductor-insulator transition in a disordered electronic system. *Phys. Rev. B* **54**, R3756-R3759 (1996).
 - [8] Sherman, D. et al. The Higgs mode in disordered superconductors close to a quantum phase transition. *Nature Physics* **11**, 188-192 (2015).
 - [9] Mondal, M. et al. Phase fluctuations in a strongly disordered s-wave NbN superconductor close to the metal-insulator transition. *Phys. Rev. Lett.* **106**, 047001 (2011).
 - [10] Matsunaga, R. et al. Light-induced collective pseudospin precession resonating with Higgs mode in a superconductor. *Science* **345**, 1145-1149 (2014).
 - [11] Cea, T., Castellani, C., Seibold, G. & Benfatto, L. Nonrelativistic dynamics of the amplitude (Higgs) mode in superconductors. *Phys. Rev. Lett.* **115**, 157002 (2015).
 - [12] Cea, T. & Benfatto, L. Nature and Raman signatures of the Higgs amplitude mode in the coexisting superconducting and charge-density-wave state. *Phys. Rev. B* **90**, 224515 (2014).
 - [13] Goldman, A. & Markovic, N. Superconductor-insulator transitions in the two-dimensional limit. *Phys. Today* **51**, 39-44 (November, 1998).
 - [14] Gantmakher, V. F. & Dolgoplov, V. T. Superconductor-insulator quantum phase transition. *Phys. Usp.* **53**, 3-53 (2010).
 - [15] Hebard, A. F. & Paalanen, M. A. Magnetic-field-tuned superconductor-insulator transition in two-dimensional films. *Phys. Rev. Lett.* **65**, 927-930 (1990).
 - [16] Kemper, A. F., Sentef, M. A., Moritz, B., Freericks, J. K. &

- Devereaux, T. P. Direct observation of Higgs mode oscillations in the pump-probe photoemission spectra of electron-phonon mediated superconductors. *Phys. Rev. B* **92**, 224517 (2015).
- [17] Measson, M.-A., Gallais, Y., Cazayous, M., Clair, B., Rodiere, P., Cario, L. & Sacuto, A. Amplitude Higgs mode in the 2H-NbSe₂ superconductor, *Phys. Rev. B* **89**, 060503(R) (2014).
- [18] Endres, M., Fukuhara, T., Pekker, D., Cheneau, M., Schauss, P., Gross, C. Demler, E., Kuhr, S. & Bloch, I. The Higgs amplitude mode at the two-dimensional superfluid/Mott insulator transition. *Nature* **487**, 454-458 (2012).
- [19] Diener, R. B., Sensarma, R. & Randeria, M. Quantum fluctuations in the superfluid state of the BCS-BEC crossover. *Phys. Rev. A* **77**, 023626 (2008).
- [20] Sacepe, B., Chapelier C., Baturina, T. I., Vinokur, V. M., Baklanov, M. R. & Sanquer, M. Disorder induced inhomogeneities of the superconducting state close to superconductor-insulator transition. *Phys. Rev. Lett.* **101**, 157006 (2008).
- [21] Randeria, M. T., Feldman, B. E., Drozdov, I. K. & Yazdani, A. Scanning Josephson Spectroscopy on atomic scale. *Phys. Rev. B* **93**, 161115(R).
- [22] Sachdev, S. *Quantum Phase Transitions* (Cambridge Univ. Press, 2001).
- [23] We note that our formalism calculates the correlators in real frequencies analytically and does not suffer from issues of analytic continuation.
- [24] E_{gap} is the gap to the single particle Fermionic excitations, and $2E_{gap}$ is the threshold for continuum of 2-particle excitations. We restrict the integral upto $2E_{gap}$ so that only contribution of collective modes are considered.
- [25] Gazit, S., Podolsky, D. & Auerbach, A. Fate of the Higgs mode near quantum criticality. *Phys. Rev. Lett.* **110**, 140401 (2013).
- [26] Cheng, B., Wu, L., Laurita, N. J., Singh, H., Chand, M., Raychaudhuri, P. & Armitage, N. P. Anomalous gap-edge dissipation in disordered superconductors on the brink of localization. *Phys. Rev. B* **93**, 180511 (2016).
- [27] Kogar, A., Rak, M. S., Vig, S., Husain, A. A., Flicker, F., Joe, Y., Luc Venema, MacDougall, G. J., Chiang, T. C., Fradkin, E., Wezel J. V. & Abbamonte, P. Signatures of exciton condensation in a transition metal dichalcogenide. *Science* **358**, 1314-1317 (2017).
-

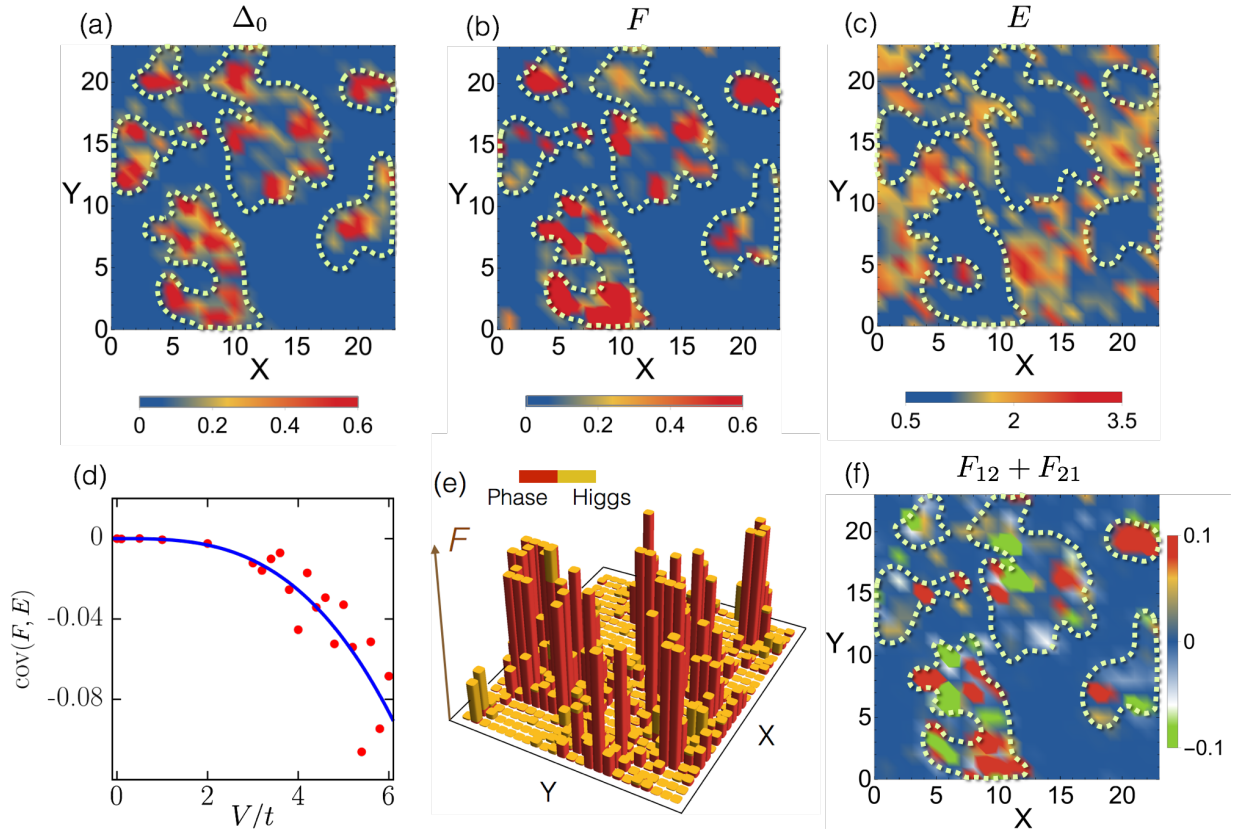


FIG. 1. Spatial maps for a particular disorder configuration at $V = 6t$ showing strong correlation between (a) the local superconducting order parameter $\Delta_0(r)$ and (b) the frequency-integrated local 2-particle spectral weight $F(r)$. (c) Spatial map of the corresponding single particle gap $E(r)$ obtained from the local 1-particle density of states [See SM for details]. Notice the strong anticorrelation between (c) and (b). (d) Covariance between $F(r)$ and $E(r)$, averaged over disorder realizations, as a function of disorder strength. The anticorrelation increases with disorder. (e): A bar map showing the relative weights of the Higgs (amplitude) and Goldstone (phase) modes in the two-particle spectral weight $F(r)$ shown in (b). The spectral weight at large disorder is dominated by the phase modes. (f) The integrated amplitude-phase mixing two-particle spectral weight $F_{12}(r) + F_{21}(r)$ corresponding to the configuration shown in (b). The mixing contribution shows regions with positive and negative values on a scale much smaller than the superconducting coherence length.

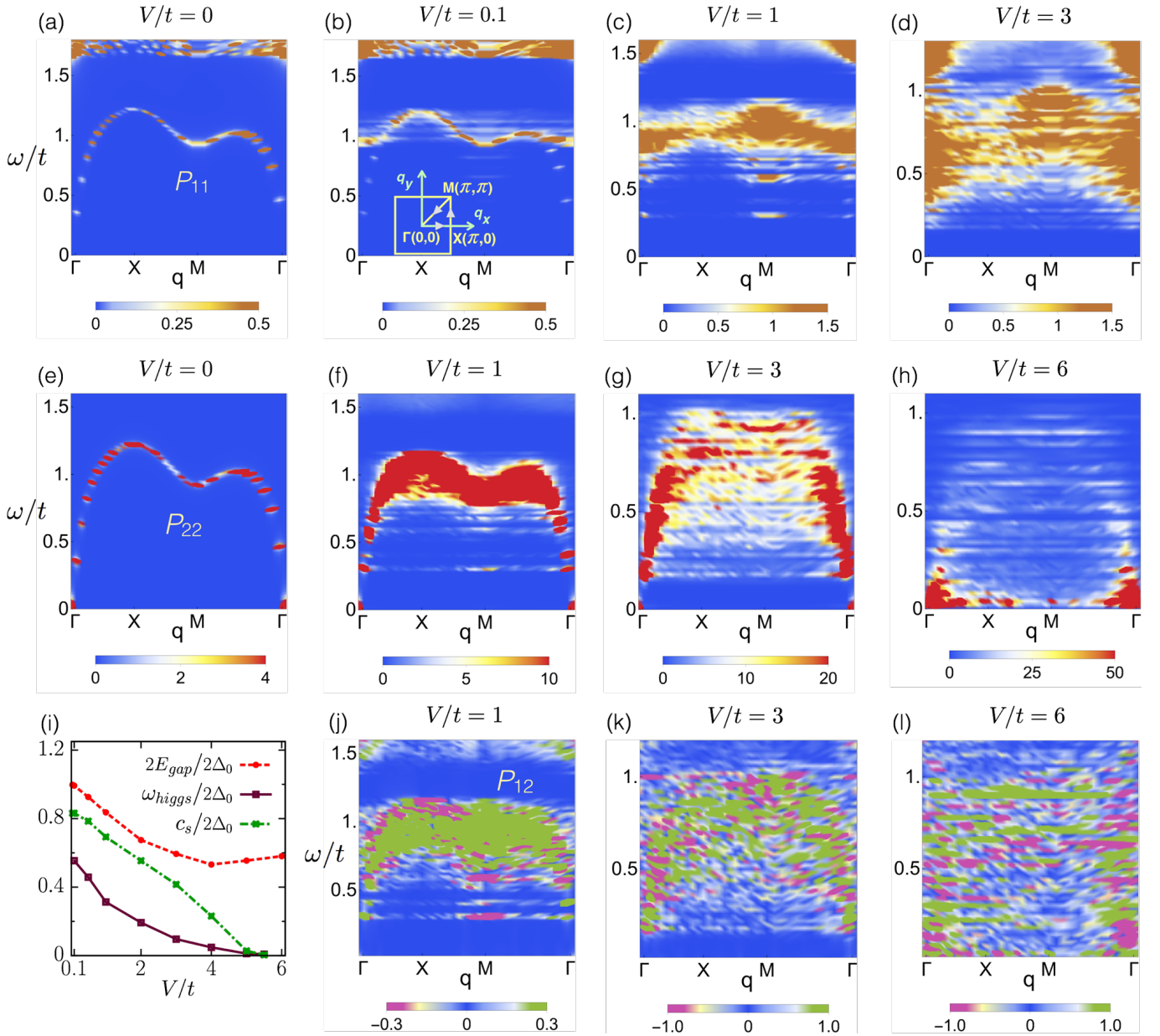


FIG. 2. (a)-(d): Higgs spectral function $P_{11}(q, \omega)$ [Eqn. 2] shown as a density plot in q and ω with increasing disorder: (a) $V = 0.0t$ showing no weight at $q = 0$; (b) weak disorder $V = 0.1t$ starts showing finite $q = 0$ weight of the Higgs mode; (c) $V = 1.0t$ and (d) $V = 3.0t$. (e)-(h): Goldstone or phase spectral function $P_{22}(q, \omega)$ [Eqn. 2] shown as a density plot in q and ω for (e) $V = 0.0t$ (f) $V = 1.0t$ (g) $V = 3.0t$ and (h) $V = 6.0t$. Note the relative stability of dispersive modes up to large disorder strength. (i) The Higgs threshold ω_{higgs} , the speed of sound c_s and the two particle continuum threshold $2E_{gap}$ (pair-breaking scale) as a function of V . (j)-(l): The amplitude-phase mixed two-particle spectral function $P_{12} + P_{21}$ [Eqn. 2] shown as a density plot as a function of q and ω for (j) $V = 1.0t$ (k) $V = 3.0t$ and (l) $V = 6.0t$. Note that the mixing term grows in magnitude but oscillates in sign more rapidly as disorder is increased leading to cancellations in measurable response functions.

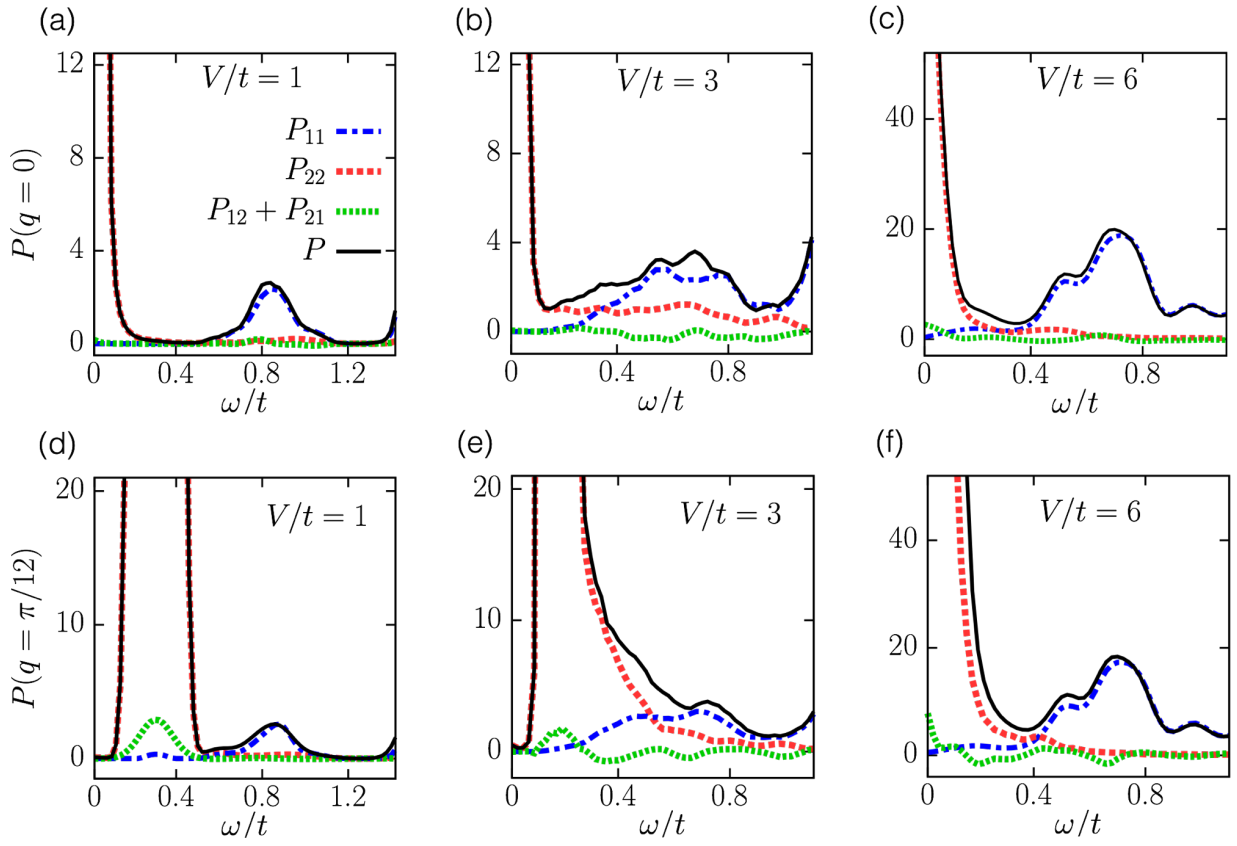


FIG. 3. Energy dependence of the spectral function P for increasing disorder $V = 1.0t$, $V = 3.0t$ and $V = 6.0t$ for (a)-(c): $q = [0, 0]$ and (d)-(f): $q = [\pi/12, 0]$. The decomposition of the spectral function contributions from the Higgs mode P_{11} , the phase mode P_{22} and the mixing $P_{12} + P_{21}$ is also shown. Note the negligible mixing contributions, and the spectral separation of Higgs and phase contributions. At low disorder the weight of the mixing term is similar to that of the Higgs mode, although they are spectrally separated. At larger disorder, the mixing term is weaker than the Higgs weight, and both are much smaller than the weight in the phase mode.

Supplementary Material for: Two-particle spectral function for disordered s-wave superconductors: local maps and collective modes

FUNCTIONAL INTEGRAL APPROACH

We will briefly sketch the key steps used to calculate the Higgs ($\mathcal{P}_{11}(r, r', \omega)$ in the main text) and the phase spectral function ($\mathcal{P}_{22}(r, r', \omega)$) as well as the amplitude-phase mixing

$$S = \int_0^\beta d\tau \sum_{rr', \sigma} \bar{f}_\sigma(r, \tau) [\partial_\tau \delta_{rr'} + H_{rr'}^0] f_\sigma(r', \tau) - U \sum_r \bar{f}_\uparrow(r, \tau) \bar{f}_\downarrow(r, \tau) f_\downarrow(r, \tau) f_\uparrow(r, \tau) \quad (3)$$

where $\beta = 1/T$, T being the temperature of the system. Using Hubbard-Stratanovich auxilliary field fields $\Delta(r, \tau)$ coupling to $\bar{f}_\uparrow(r, \tau) \bar{f}_\downarrow(r, \tau)$ and $\xi(r, \tau)$ coupling to $\bar{f}(r, \tau) f(r, \tau)$, and introducing the Nambu

$$S_{eff} = \int_0^\beta d\tau \sum_r \frac{|\Delta(r, \tau)|^2 + |\xi(r, \tau)|^2}{U} - \int d\tau d\tau' \sum_{rr'} \psi^\dagger(r, \tau) G^{-1}(r, \tau; r', \tau') \psi(r', \tau'), \quad \text{and} \quad (4)$$

$$G^{-1}(r, \tau; r', \tau') = \delta(\tau - \tau') \begin{pmatrix} -(\partial_\tau - \mu(r, \tau))\delta_{rr'} + t\delta_{\langle rr' \rangle} & -\Delta(r, \tau)\delta_{rr'} \\ -\Delta^*(r, \tau)\delta_{rr'} & -(\partial_\tau + \mu(r, \tau))\delta_{rr'} - t\delta_{\langle rr' \rangle} \end{pmatrix},$$

where $\mu(r, \tau) = \mu - v(r) - \xi(r, \tau)$. The static but spatially dependent saddle point profile, $\Delta(r, \tau) = \Delta_0(r)$ and $\xi(r, \tau) = \xi_0(r)$, reproduce the BdG mean field theory, with the saddle point equations $\delta S/\delta \Delta_0(r) = 0$ and $\delta S/\delta \xi_0(r) = 0$ giving the BdG self-consistency equations,

$$\Delta_0(r) = |U| \sum_n u_n(r) v_n^*(r),$$

$$\xi_0(r) = |U| \sum_n |v_n(r)|^2 \quad \text{and} \quad \langle n \rangle = \frac{2}{N_s} \sum_{n,r} |v_n(r)|^2 \quad (5)$$

$$S_G = \sum_{ij} \sum_{\omega_m} (\eta(i, \omega_m) \quad \theta(i, \omega_m)) \begin{pmatrix} D^{-1}_{11}(i, j, \omega_m) & D^{-1}_{12}(i, j, \omega_m) \\ D^{-1}_{21}(i, j, \omega_m) & D^{-1}_{22}(i, j, \omega_m) \end{pmatrix} \begin{pmatrix} \eta(j, -\omega_m) \\ \theta(j, -\omega_m) \end{pmatrix}. \quad (6)$$

where $\omega_m = (2m)\pi/\beta$ is the Bosonic Matsubara frequency. We work in the amplitude and phase degrees of freedom rather than the ‘‘Cartesian’’ co-ordinates which mix these degrees of freedom, so that we can cleanly talk about Higgs and phase

term ($\mathcal{P}_{12}(r, r', \omega)$) in the disordered s-wave superconductor within a functional integral approach. The partition function Z for the disordered negative U Hubbard model (Eqn. (1) in main paper) can be written in terms of the fermion fields ($\bar{f}_\sigma(r, \tau), f_\sigma(r, \tau)$) as $Z = \int D[\bar{f}_\sigma, f_\sigma] e^{-S[\bar{f}_\sigma, f_\sigma]}$, with the imaginary time (τ) action

spinors $\psi^\dagger(r, \tau) = \{\bar{f}_\uparrow(r, \tau), f_\downarrow(r, \tau)\}$, we get $Z = \int D[\bar{f}_\sigma, f_\sigma] D[\Delta^*, \Delta] D[\xi] e^{-S_{eff}[\bar{f}_\sigma, f_\sigma, \Delta^*, \Delta, \xi]}$, with

where $[u_n(r), v_n(r)]$ are the eigenvector of $G^{-1}(r, r', \omega)$ corresponding to eigenvalue $\omega - E_n$ and n runs over only positive eigenvalues ($E_n > 0$).

Going beyond the saddle point approximation, we include (in Eqn. (4)) the spatio-temporal fluctuations of the Δ field i.e. $\Delta(r, \tau) = (\Delta_0(r) + \eta(r, \tau)) e^{i\theta(r, \tau)}$, where $\eta(r, \tau)$ is the amplitude and $\theta(r, \tau)$ is the phase fluctuation around the saddle point solution. The fermion fields are then integrated out, and the resulting action is expanded upto quadratic order in η and θ to obtain the Gaussian action for the amplitude and phase fluctuations,

modes. The inverse propagator matrix D^{-1} is analytically continued to real frequencies. We note that we work directly in real frequencies and do not need to do numerical analytic continuation. Working at $T = 0$, the real frequency re-

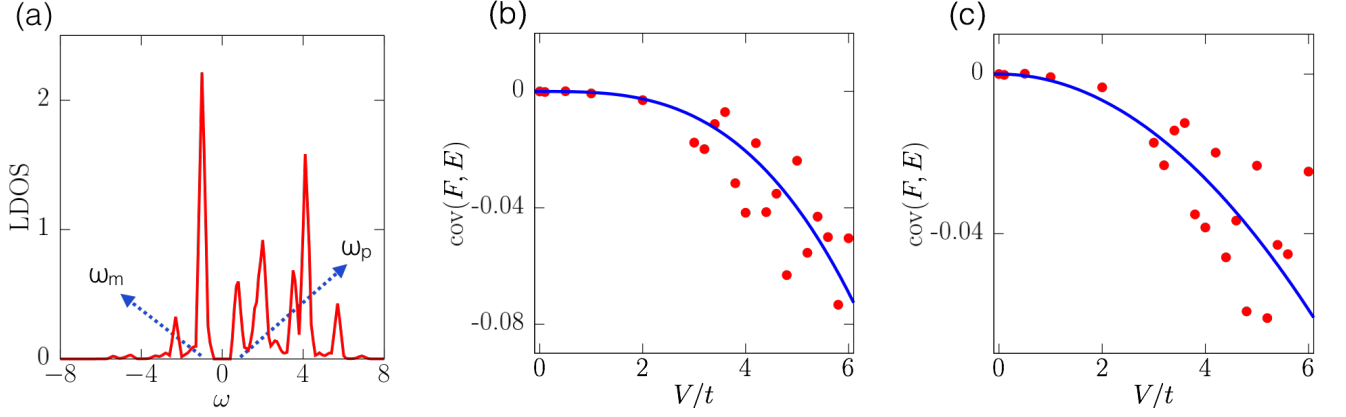


FIG. 4. (a): LDOS as a function of ω for a particular site. The locations of ω_p and ω_m are indicated in the figure. (b)-(c): Covariance between two particle spectral function (F) and local single particle gap (E) where F is defined as (b) $F(i) = \int_{0.2 \times 2E_{gap}}^{2E_{gap}} P(i, i, \omega) d\omega$ and (c) $F(i) = \int_{0.3 \times 2E_{gap}}^{2E_{gap}} P(i, i, \omega) d\omega$.

tarted inverse fluctuation propagators $D^{-1}_{\alpha\beta}(i, j, \omega)$ in terms of BdG eigenvalues and eigenfunctions can be written as:

$$D_{11}^{-1}(r, r', \omega) = \frac{1}{U} \delta_{rr'} + \frac{1}{2} \sum_{E_{n,n'} > 0} f_{nn'}^1(r) f_{nn'}^1(r') \chi_{nn'}(\omega) \quad (7)$$

where $f_{nn'}^1(r) = [u_n(r)u_{n'}(r) - v_n(r)v_{n'}(r)]$ and $\chi_{nn'}(\omega) = (\omega + i0^+ - E_n - E_{n'})^{-1} - (\omega + i0^+ + E_n + E_{n'})^{-1}$. The off diagonal element is given by

$$D_{12}^{-1}(r, r', \omega) = -\frac{i\omega}{4} \sum_{E_{n,n'} > 0} f_{nn'}^1(r) f_{nn'}^2(r') \chi_{nn'}(\omega) \quad (8)$$

where $f_{nn'}^2(r) = [u_n(r)v_{n'}(r) + v_n(r)u_{n'}(r)]$ and

$$D_{22}^{-1}(r, r', \omega) = \tilde{D}_{dia}(r, r') + \omega^2 \kappa(r, r', \omega) + \Lambda(r, r', \omega) \quad (9)$$

where the diamagnetic piece $\tilde{D}_{dia} = 2 \sum_{\langle rr_1 \rangle} S(r, r_1)$ for $r = r'$, $\tilde{D}_{dia} = -2S(r, r')$ when r and r' are nearest neighbours, and 0 otherwise, where $S(r, r') = \frac{t}{4} \sum_{E_n > 0} v_n(r)v_n(r')$, and the compressibility

$$\kappa(r, r', \omega) = \frac{1}{8} \sum_{E_{n,n'} > 0} f_{nn'}^2(r) f_{nn'}^2(r') \chi_{nn'}(\omega) \quad (10)$$

Finally the paramagnetic current-current correlator on the lattice, $\Lambda(r, r', \omega)$ is given by the expression

$$\Lambda(r, r', \omega) = \sum_{\langle rr_1 \rangle \langle r'r_2 \rangle} J(r, r_1, r', r_2, \omega) - J(r, r_1, r_2, r', \omega) - J(r_1, r, r', r_2, \omega) + J(r_1, r, r_2, r', \omega) \quad (11)$$

where

$$J(r, r_1, r', r_2, \omega) = -\frac{t^2}{8} \sum_{n, n'} f_{nn'}^3(r, r') f_{nn'}^3(r_2, r_1) \chi_{nn'}(\omega) \quad (12)$$

where $f_{nn'}^3(r, r') = [u_n(r)v_{n'}(r') - v_n(r)u_{n'}(r')]$.

We construct the inverse propagators in real space (continued to real frequency), invert the matrix to obtain the propagators $D_{\alpha\beta}(r, r', \omega)$ and spectral functions, $\mathcal{P}_{\alpha\beta}(i, j, \omega) = -\frac{1}{\pi} \text{Im} D_{\alpha\beta}(i, j, \omega)$ in real space for each disorder configuration. This is then Fourier transformed to obtain the spectral functions in (q, ω) and then a disorder averaging is performed over relevant quantities.

LOCAL SINGLE PARTICLE GAP

In this section we provide the details of our method to obtain the local gap map, which is also used to show anti-correlation between one particle gap and two particle spectral weight in the system. The local single particle density of states (LDOS) for each site i , calculated from BdG MF theory, is given by

$$N_\omega(r) = \frac{1}{N_s} \sum_n u_n^2(r) \delta(\omega - E_n) + v_n^2(r) \delta(\omega + E_n). \quad (13)$$

The local single particle gap $E(r)$ for each site r is obtained from $E(r) = \frac{\omega_p(r) - \omega_m(r)}{2}$, where $\omega_p(r)$ is the location of the lowest energy peak in LDOS for $\omega > 0$ and $\omega_m(r)$ is the location of the highest energy peak in LDOS for $\omega < 0$. In Fig. 4(a) we have shown a sample LDOS for a particular site. The figure also shows the location of $\omega_p(r)$ and $\omega_m(r)$ for this site and the corresponding local gap $E(r)$ obtained from this LDOS.

**COVARIANCE BETWEEN SINGLE PARTICLE GAP AND
TWO PARTICLE SPECTRAL FUNCTION**

To understand the spatial variation for the local two particle spectral function ($P(i, i, \omega)$), we consider the integrated spectral weight of P , $F(i) = \int_0^{2E_{gap}} P(i, i, \omega) d\omega$. We calculate the covariance between two experimentally observable quantities namely two particle spectral function (F) and local single particle gap (E) as

$$\text{cov}(F, E) = \langle FE \rangle - \langle F \rangle \langle E \rangle. \quad (14)$$

In Fig. 4(b) and (c) we show the covariance between F and E as a function of disorder, where F has been calculated with different integration limits, $F(i) = \int_{0.2 \times 2E_{gap}}^{2E_{gap}} P(i, i, \omega) d\omega$ and $F(i) = \int_{0.3 \times 2E_{gap}}^{2E_{gap}} P(i, i, \omega) d\omega$ respectively. We find that with increasing the lower cut-off of the integration the anti-correlation between F and E at large disorder persists but it becomes weaker.